ELSEVIER

Materials Chemistry and Physics 54 (1998) 60–66

MATERIALS CHEMISTRY AND PHYSICS

Controlling the diffusion of implanted boron in Si and silicide by multiple implants

Chih-Hsun Chu [a,*], Kwhy-Jrung Ho [b], Cheng-Tung Huang [c], Shin-Huey Shvu [c], Tan-Fu Lei [c]

[a] *Mosel Vitelic Inc., Hsinchu, Taiwan*

[b] *Department of Chemistry, National Tsing Hua University, Hsinchu, Taiwan*

[c] *Institute of Electronics, National Chiao Tung University, Hsinchu, Taiwan*

Abstract

To form an ultra-shallow p^+-n junction by direct low energy BF_2^+ implantation is difficult. The channeling of the boron during implant and the transient enhanced diffusion of boron during annealing prohibit the tight control of the boron profile. Using the germanium pre-amorphization implant, the channeling probability of the boron is suppressed. However, the thickness of the pre-amorphized layer is crucial in alleviating the transient enhanced diffusion of boron. The excess point defects below the original amorphous/crystalline interface play a key role in enhancing the diffusion of boron. Introducing the carbon into the BF_2^+ implanted Si, the diffusion of the boron is retarded. Combining with the germanium pre-amorphization implant, low energy BF_2^+ implant and carbon implant, an ultra-shallow p^+-n junction with a junction depth of about 70 nm is realized after rapid thermal annealing at 1050°C, 10 s. Using the boron implanted $TiSi_2$ as diffusion source to form an ultra-shallow p^+-n junction is prohibited by the trapping of boron inside the $TiSi_2$. The fabrication of high quality p^+-n junction using this technique is difficult to achieve. Incorporation of germanium into the boron containing $TiSi_2$, the diffusion of boron inside the $TiSi_2$ is enhanced. Boron easily out-diffuses from the $TiSi_2$ layer into the Si substrate and forms a high quality p^+-n shallow junction. Manipulating the diffusion behavior of implanted boron in the Si and $TiSi_2$ could be achieved by the multiple implants of germanium and carbon. The chemical interaction of co-implanted ions with the boron is the key to control the boron profile inside the silicon.

Keywords: Ultra-shallow p^+/n junction; Ge^+ preamorphization; Low energy BF_2^+ implant; Carbon co-implant; Diffusion

1. Introduction

The advancement of the integrated circuits fabrication technology pushes the scaling of the device. According to the subthreshold scaling rule [1], the junction depth will be in the sub-0.1 μm regime as the gate length approaching 0.1 μm. A large number of methods have been proposed to fabricate the ultra-shallow junction [2–6]. The simple and direct approach is to use low energy implantation. However, considering the contact formation on the ultra-shallow junction, silicide as a diffusion source (SADS) is an attractive alternative [5]. Both methods on the ultra-shallow p^+/n junction formation meet some challenges. The diffusivity of the boron is enhanced and retarded in direct implant and SADS processes, respectively. These unwanted phenomena prove to be obstacles to achieve an ultra-shallow p^+/n junction.

To form such ultra-shallow p^+/n junction by direct ion implantation, ion channeling during ion implantation and transient enhanced diffusion of dopant during post-implantation annealing need to be alleviated. Previously, promising results have been reported in low energy Ge^+ pre-amorphized and BF_2^+ implanted silicon [6]. In this case a thin amorphous layer which is thinner than the implant profile is formed. The excess point defects below the original amorphous/crystalline (a/c) interface will interact with the boron and enhance boron diffusion during post-implantation annealing. A complete solution to these problems is to form a thicker amorphous layer which is much deeper than the junction depth. The thickness of the amorphous layer (X_α) has to be larger than the sum of the junction depth (X_j), depletion region width (W_d) and width of residual defect region (X_r). In addition, the size, density and distribution of the residual defects formed near the original (a/c) interface need to be reduced.

* Corresponding author. Progress Integration Department, United Silicon Inc. No. 3, Li-Hsin Rd. 2, Science-based Industrial Park, Hsinchu, Taiwan. Tel.: +886-3-5789388; Fax: +886-3-5789758; E-mail: Chih Hsun Chu@usic.com.tw

0254-0584/98/$19.00
PII S0254-0584(98)00016-9

Carbon implantation into boron implanted silicon shows retarded boron diffusion inside an amorphous silicon layer and lower defect density near the original a/c interface [7]. It is an appropriate candidate to control the boron diffusion in the deep germanium pre-amorphized and BF_2^+ implanted silicon to overcome the problems induced by the original a/c interface and fast diffusion of boron.

Another approach to achieve the ultra-shallow junction is to use doped silicide as a diffusion source (SADS) [5]. In this way good silicide contacted ultra-shallow junction could be formed at the same time. However, for boron implanted $TiSi_2$, it is difficult for boron to diffuse from the $TiSi_2$ into the silicon substrate due to the formation of TiB_2 compound inside the $TiSi_2$ layer [8–11]. During the formation of $TiSi_2$ on p-type silicon, the boron inside the silicon substrate segregates into the $TiSi_2$ and causes surface depletion of boron [12]. To solve these problems, Ge^+ implantation into the $TiSi_2$, with all the Ge atoms located inside the $TiSi_2$, was conducted to enhance the out diffusion of boron.

2. Experimental

Conducting direct implant to form p^+/n ultra-shallow junction, n-type (001)Si wafers were pre-amorphized by Ge^+ implantation with various energies and were doped by low energy (5 keV) BF_2^+ implantation to a dose of 5×10^{14} cm^{-2}. The implant conditions are listed in Table 1. In Table 1, Ref denotes the control sample that receives 5 keV BF_2^+ implant. The Sa, La, Ma and Da stand for shallow, light, medium and deep pre-amorphization, respectively. Post-implantation annealing was carried out in furnace and rapid thermal annealing (RTA) system. The annealing conditions are listed in Table 2. TRIM code [13] was utilized to calculate the damage production and energy deposition in silicon during Ge^+ pre-amorphization and C^+ implants.

Table 1
Implantation conditions for multiple implants

Implant condition	Ref	Sa	La	Ma	Da	C95	C150	C250	C500
BF_2^+, 5 keV, 5×10^{14} cm^{-2}	*	*	*	*	*	*	*	*	*
Ge^+, 5 keV, 5×10^{14} cm^{-2}		*							
Ge^+, 30 keV, 5×10^{14} cm^{-2}			*		*	*	*	*	*
Ge^+, 200 keV, 5×10^{14} cm^{-2}				*	*	*	*	*	*
Ge^+, 400 keV, 1×10^{14} cm^{-2}					*	*	*	*	*
C^+, 95 keV, 2×10^{15} cm^{-2}						*			
C^+, 150 keV, 1×10^{15} cm^{-2}							*		
C^+, 250 keV, 1×10^{15} cm^{-2}								*	
C^+, 500 keV, 1×10^{15} cm^{-2}									*

Table 2
Annealing conditions of the multiple implanted samples

Thermal cycle (°C)	600	900	1050
RTA (s)		10	10
Furnace (min)	30	10	
Furnace + RTA	30	10	

For using SADS to form p^+/n ultra-shallow junction, 65 nm $TiSi_2$ was formed on top of substrate by the reaction of Ti (50 nm) and α-Si (5 nm) layers at 625°C for 20 min. The unreacted Ti and TiN were removed by wet etching selectively. Ge^+ and B^+ were implanted into the $TiSi_2$ layer with an energy and dose of 60 keV, 5×10^{14} cm^{-2} and 10 keV, 5×10^{15} cm^{-2}, respectively. The energies of Ge^+ and B^+ implants were chosen so that all the ions were located inside the $TiSi_2$ layer. The drive-in process was carried out at 800–950°C for 15 min in N_2 ambient to form C54-$TiSi_2$ and p^+/n junction simultaneously.

The microstructure and boron depth profile of the as-implanted and annealed samples were investigated by transmission electron microscopy (TEM) and secondary ion mass spectrometry (SIMS), respectively. The junction leakage of the Ti silicided diode was characterized by the *I–V* measurement.

3. Results and discussion

3.1. Boron diffusion in Ge pre-amorphized BF_2^+ implanted silicon

Using the direct implant to form the ultra-shallow p^+/n junction, the boron channeling phenomena and transient enhanced diffusion have to be eliminated. Utilizing the screen layer to dechannel the low energy boron ions is not practical due to the loss of dopant inside the screen layer. Using an isoelectronic ion implant to pre-amorphize the silicon substrate before conducting the doping implant is an easy and straightforward approach to suppress the boron channeling. However, for common practice, the amorphous layer induced by the pre-amorphization implant is thinner than the p^+ layer. The excess interstitials underneath the a/c interface enhance the diffusion of boron during the post-implant annealing causing transient enhanced diffusion. In order to eliminate both the ion channeling and transient enhanced diffusion, a deep pre-amorphization implant is conducted to generate a thick amorphous layer which is thicker than that of the p^+ layer. In this case, implanted boron atoms are all located inside the amorphous layer. The junction of p^+/n is also located inside the amorphous layer. No excess interstitials are available to enhance the boron diffusion. The depth distributions of as implanted boron measured by SIMS from different samples

are plotted in Fig. 1. The impact energy of O_2^+ ion is 3 keV to reduce the profile broadening effect and oxygen flooding on the surface is utilized to suppress the surface transient region. The probability of boron channeling in the Ref sample is higher than that of the rest of the samples. The boron depth profiles of samples pre-amorphized by germanium implantation at different energies exhibit no significant difference as shown in Fig. 1. The thickness of the amorphous layers measured by cross-sectional transmission electron microscopy (XTEM) is listed in Table 3. During this low energy (5 keV) BF_2^+ implant, the amorphization of surface layers by various Ge^+ implants shows a similar effect on the suppression of the boron channeling.

After furnace annealing at 600°C for 30 min, the depth distributions of boron are almost unchanged as compared with as-implanted profiles, as shown in Fig. 2. From the XTEM investigation, point defect clusters were found below the original a/c interface. In samples with a thin amorphous layer such as Ref, Sa and La samples, a low density of small point defect clusters were observed near the original a/c interface. Thin amorphous layer created by the implant in Ref, Sa and La samples can be fully recovered without end-of-range defects left after 900°C, 10 min annealing. The removal of the end-of-range defects in the shallow implant is attributed to the proximity of the a/c interface to the free surface which provides a sufficient amount of vacancies with short diffusion path to recombine with the excess interstitials and to a lesser amount of excess interstitials generated during low energy BF_2^+ implant and shallow Ge^+-pre-amorphization implant.

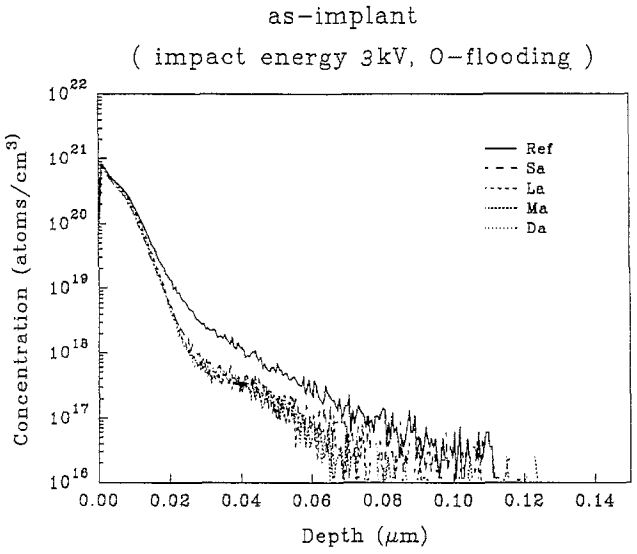

Fig. 1. SIMS depth profile of boron in the as-implanted samples.

Table 3
Thickness of the amorphous layers induced by the implant

Sample	Ref	Sa	La	Ma	Da
Thickness (nm)	6.5	17	42	195	230

After RTA at 1050°C, 10 s, boron redistributions were observed from the SIMS analysis, as shown in Fig. 3. The Da sample has the shallowest boron distribution. The junction depth measured by the interception of the boron depth profile with the concentration of 10^{17} cm^{-3} is 70 nm in sample Da. The Ma and La samples have the deepest distribution of boron. The junctions of La and Ma are all deeper than 0.11 μm. The depth profile of boron in the Sa sample is shallower than that of the Ref sample. The junction depths of the Sa and Ref samples are 0.08 μm and 0.095 μm, respectively. In the La sample, the junction depth is deeper than the original a/c interface (0.042 μm). While in the Ma sample, the junction depth is shallower than the original a/c interface (0.195 μm). The presence of the excess interstitials may be the cause of the resultant enhanced boron diffusion in the La sample, and the residual defects near the original a/c interface may attract the boron and deepen the junction in the Ma sample. In the Sa sample, the original a/c interface

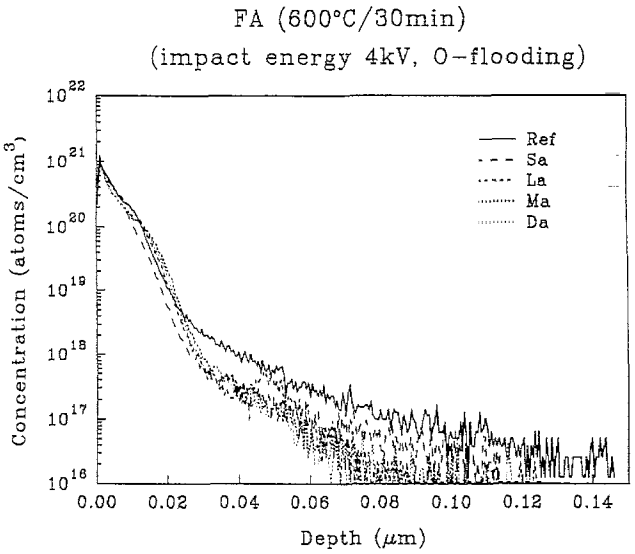

Fig. 2. SIMS depth profile of boron in the 600°C, 30 min annealed samples.

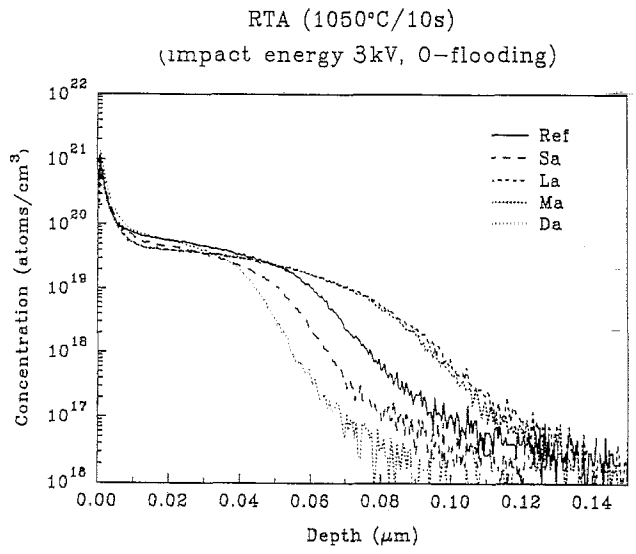

Fig. 3. SIMS depth profile of boron in the 1050°C, 10 s annealed samples.

(0.017 μm) is far away from the junction and the channeling is lighter than that of the Ref sample. In the deep amorphized Da sample, the original a/c interface is the deepest. Both the ion channeling and transient enhanced boron diffusion are suppressed.

3.2. Boron diffusion in Ge pre-amorphized and BF_2^+, C^+ co-implanted silicon

Retarded boron diffusion inside the amorphous silicon and lowered residual defect density near the original a/c interface have been reported in the carbon implanted silicon [7]. It is a primary candidate for ion beam defect engineering (IBDE) to overcome the problems induced by the original a/c interface. Two types of carbon implants were performed. Type I is to coincide the projected range of carbon implant with the original a/c interface formed by the Ge^+ pre-amorphization in Da sample. Type II is to place the projected range of the carbon far beyond the original a/c interface so that the excess vacancy region of carbon implant overlapped with the excess interstitial region of Ge^+ pre-amorphization implant. The design of carbon implant condition is crucial to the suppression of boron diffusion and defect reduction. Before performing the carbon implant, the amorphous layer thickness of the sample needs to be known. The formation of the amorphous layer is related to the energy deposition during the ion implant. To predict the thickness of the amorphous layer, the threshold energy used to form the amorphous layer needs to be determined. The results of TRIM cascade calculation can be calibrated by XTEM to obtain the threshold energy of amorphization in Ge^+ implanted silicon. Fig. 4 is the energy deposition distributions in the Ge^+ pre-amorphized samples calculated from TRIM code at different combination of implant energies. The thickness of the amorphous layers measured by XTEM is also denoted. The threshold energy used to form the amorphous layers in Ge^+ implanted silicon is determined to be 1.06×10^{24} eV cm^{-3}.

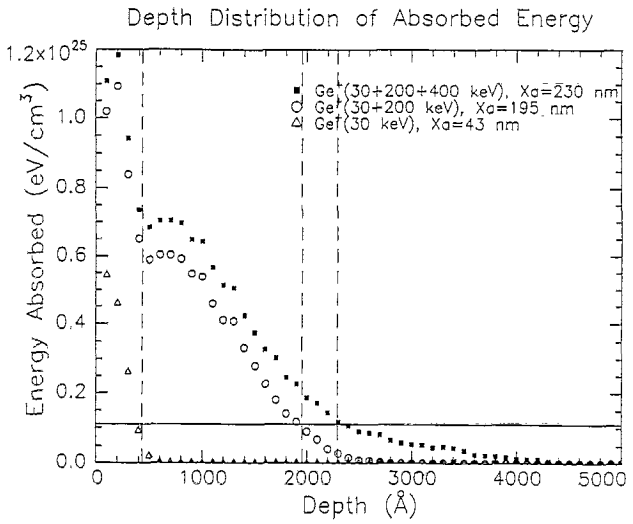

Fig. 4. The energy deposition distributions in Ge^+ pre-amorphized samples calculated from TRIM code at a different combination of implant energies.

In type I implant, the projected range of carbon was designed to coincide with the original a/c interface. The carbon distribution can be simulated by TRIM calculation. Based on the amorphous layer thickness obtained from the energy deposition distribution calculated from TRIM, the energy of carbon implant was determined. For Da samples with an amorphous layer of 230 nm, the carbon implant energy is about 95 keV. Two types of residual defects were observed from the plane view samples by TEM as shown in Fig. 5(b). Dislocation loops and defect clusters were observed to be the predominant defects. Comparing the results with the reference sample (Da) as shown in Fig. 5(a), the density of the dislocation loops is about 1/3 of the reference sample and the average size is about 10 nm. Boron depth profiles of type I carbon implanted samples are shown in Fig. 6. From the profile measured by the SIMS, retarded diffusion of boron is clearly seen. In the type I implant, the implanted carbon atoms interact with boron and silicon interstitials and result in the retardation of the boron diffusion and reduction in the size of the residual defects. Type I implant provides a better control of boron profile and reduces the size and density of the residual defects near the original a/c interface. However, the carbon implant should not degrade the sharpness of the original a/c interface. The maintenance of the sharpness of the a/c interface will alleviate the formation of hair-pin dislocations which penetrate through the regrowth layer and short the junction.

In type II implant, the distribution of excess interstitial is a key parameter needed to conduct the IBDE implant. During the ion implantation, vacancies and interstitials are generated

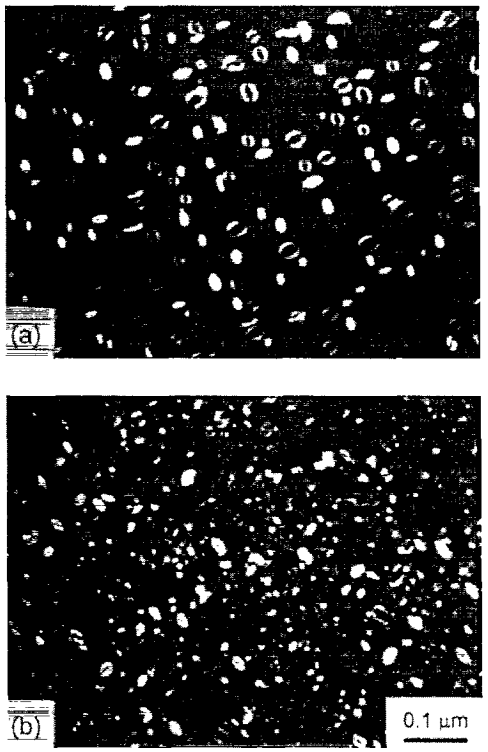

Fig. 5. Plane view TEM images of (a) Da, and (b) C95 samples annealed at 900°C, 10 min.

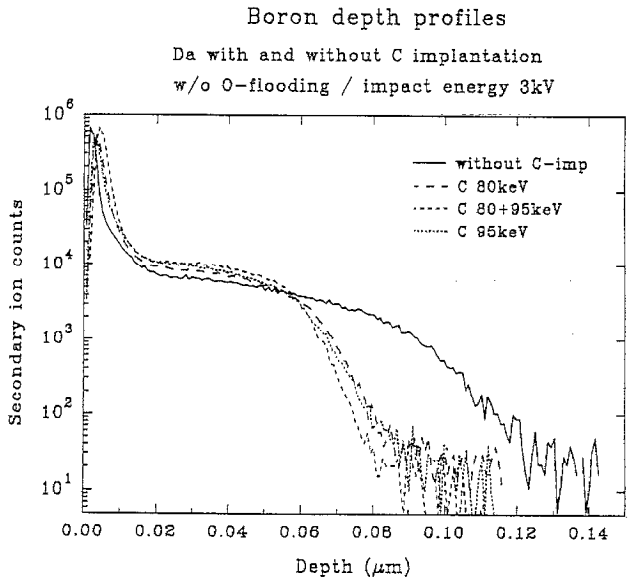

Fig. 6. The effect of type I carbon implant on the boron depth profiles in 900°C, 10 min annealed Da samples. Retardation of boron diffusion is clearly observed.

inside the silicon along the penetration path of implanted ions. Residual defects are formed by the coalescence of point defects during the post-implantation annealing. The distribution of excess interstitial calculated by TRIM is shown in Fig. 7 for samples Da, C250 and 250 keV C^+ implant to a dose of 10^{15} cm^{-2}. The thickness of the amorphous layer is about 230 nm in the Da sample. Inside the amorphous region, excess point defects are hard to define. Our interest will be concentrated on the region below the a/c interface. From the results shown in Fig. 7, carbon implant is not an efficient way to generate excess vacancies to recombine with silicon interstitials generated by the Ge^+ pre-amorphization. However, the disordering induced by the carbon implant in the much deeper depth attracts the excess interstitials beneath the original a/c interface and reduce the size of the residual defects

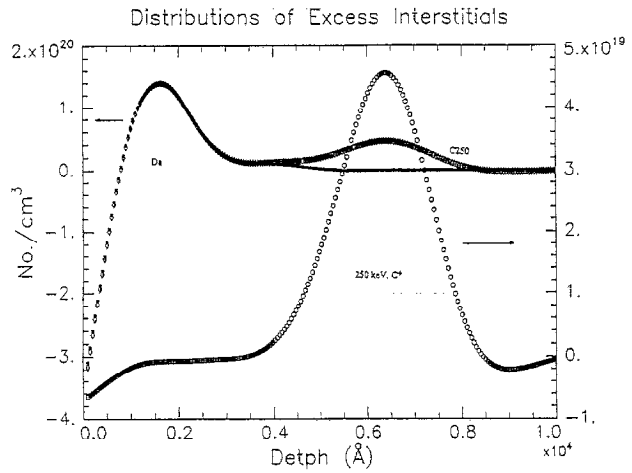

Fig. 7. The distribution of excess interstitials calculated by TRIM for Da, C250 and 250 keV C^+ implant to a dose of 10^{15} cm^{-2}.

near the original a/c interface, as shown in Fig. 8. In addition to the hair-pin dislocations in the regrowth layer, residual defects near the a/c interface are separated into two layers. At the original a/c interface, instead of dislocation loops, small defect clusters were formed. Beneath the original a/c interface, formation of dislocation loops were observed. The effect of type II implant on the boron depth profile is shown in Fig. 9. Increasing the energy of the carbon implant lessens the retardation of boron diffusion. Inducing heavy disordering deep inside the silicon substrate to reduce the excess interstitials near the original a/c interface is, therefore, the main advantage of the type II implant.

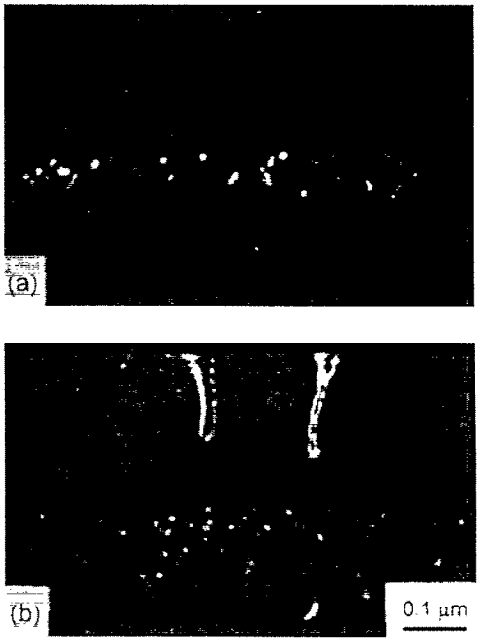

Fig. 8. Cross-sectional TEM image of (a) Da, and (b) C150 samples annealed at 900°C, 10 min.

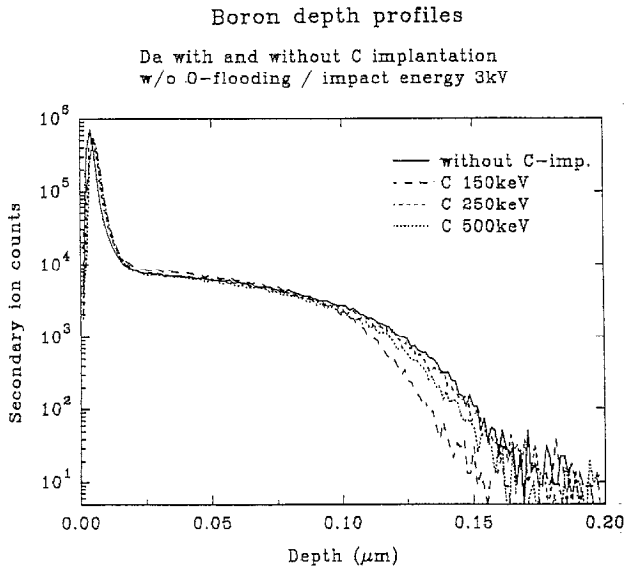

Fig. 9. The effect of type II carbon implant on the boron depth profile in 900°C, 10 min annealed Da samples.

3.3. Boron diffusion in Ge^+ implanted $TiSi_2$

More boron atoms were observed to diffuse from the Ge implanted $TiSi_2$ into the silicon substrate as compared with the sample without Ge implant, as shown in Fig. 10. The dopant redistributions were measured after removing the silicide layer and TiB by dipping in dilute HF and $NH_4OH/H_2O_2/H_2O$ solutions, respectively. The surface concentration of boron in a Ge^+ implanted sample is about three times higher than that in the control sample. The amount of out-diffused boron increases with the drive-in temperature. The reverse current densities (J_r) at -5 V reverse bias were plotted as a function of the drive-in temperatures, as shown in Fig. 11. Before the agglomeration of the $TiSi_2$ at high temperature, the leakage current of the SADS fabricated p^+/n junction with Ge^+ implant is less than 1 nA cm^{-2} and shows tight distribution. The leakage currents of the conventional SADS fabricated p^+/n junction were in a range between 2–10 nA cm^{-2}. The ideality factor n of the Ge^+ implanted diodes is ≤ 1.001 over 7 decades in a log scale. The reverse leakage composes of diffusion and generation components. The temperature dependence of the junction current is shown in Fig. 12. From the slope of the $\log(J_s/T^3)$ versus $1/T$ reveals the activation energy of the leakage current. For conventional SADS diodes, a distinct change of slope (from 1.01 to 0.68 eV) is observed at 90°C, which indicates the change of dominate component of leakage. In Ge^+ implanted SADS diodes, a constant activation energy of 1.03 eV is measured, which is fairly close to the silicon bandgap energy of 1.12 eV. It is clear that the diffusion current is the dominant component of reverse leakage current in the Ge^+ implanted SADS diodes.

In the conventional SADS process, the out diffusion of boron from the $TiSi_2$ is very difficult [8,9]. The well-known immobility of B in $TiSi_2$ is due to the precipitation of TiB_2. The heat of formation of the TiB_2 is -324 kJ mol^{-1}, which is larger than that of the $TiSi_2$ (-134 kJ mol^{-1}). TiB_2 is more stable than $TiSi_2$ and has an extremely high melting point. TiB_2 is easily formed inside the boron contained $TiSi_2$ which consumes most of the boron [8,9]. The solid solubility of boron in the $TiSi_2$ system is so low that limited amount of boron inside the $TiSi_2$ is available as a mobile dopant to diffuse into the Si substrate. The formation of the TiB reduces the dopant concentration beneath the $TiSi_2/Si$ interface causing the depletion of boron in the silicon surface.

The incorporation of Ge into the $TiSi_2$ enhances the boron diffusion. This effect not only may be due to the physical effect (pre-amorphization of the $TiSi_2$) but also may be due to the chemical effect (interaction of boron with Ge). Ge is reported to have high diffusivity and solubility inside the $TiSi_2$ [14]. The diffusivity of Ge in the $TiSi_2$ film is faster as compared with other dopants, such as P, As, B, and Sb atoms [14]. The interactions between Ti–B, Ti–Ge, Ge–B affect the diffusion behavior of boron in the Ge^+ implanted $TiSi_2$. The formation of the Ti–Ge compound releases the trapping of the boron by the Ti atoms. Without trapping by the Ti atom, boron is free to diffuse. Interstitial and substitutional B are reported to be trapped and fast diffuse in the high Ge concentration area, respectively [15]. The Ge–B interaction enhance the boron diffusion inside the Ge^+ implanted $TiSi_2$. Both the suppression of the formation of TiB_2 and enhanced boron diffusion due to the addition of the mobile Ge atoms make the formation of ultra-shallow p^+/n junction by the SADS process possible.

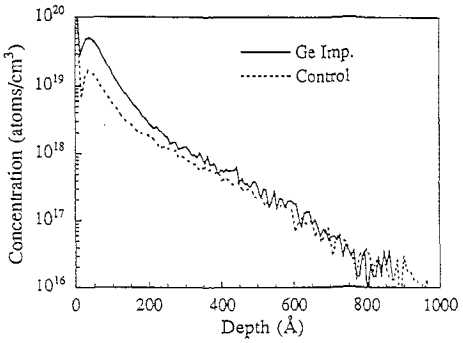

Fig. 10. SIMS depth profiles of boron in Si from samples with Ge^+ and B^+ implanted $TiSi_2$ samples, and the conventional B^+ implanted $TiSi_2$ samples.

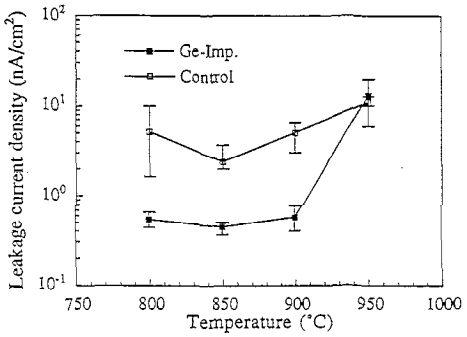

Fig. 11. The reverse current densities (J_r) at -5 V reverse bias as a function of the drive-in temperatures in Ge^+ and B^+ implanted $TiSi_2$ samples, and the conventional B^+ implanted $TiSi_2$ samples.

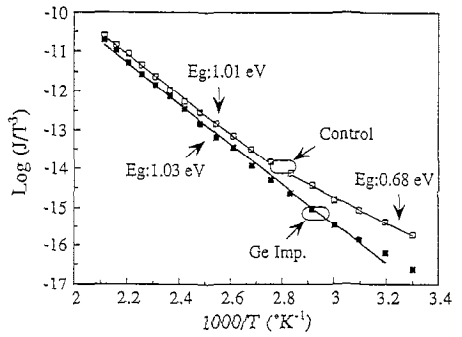

Fig. 12. The temperature dependence of the junction leakage current in Ge^+ and B^+ implanted $TiSi_2$ samples, and the conventional B^+ implanted $TiSi_2$ samples.

4. Conclusions

In summary, ultra-shallow boron profiles have been successfully achieved by the Ge^+ pre-amorphization and low

energy BF_2^+ implant with or without the carbon co-implant. Ultra-shallow p^+/n diodes fabricated by the SADS process with Ge^+ and B^+ implanted $TiSi_2$ show excellent *I–V* characteristics and low junction leakage. TRIM cascade calculation has been utilized to analyze the defect production and energy deposition in the ion implanted silicon. Prediction of the thickness of the amorphous layer induced by the Ge^+ pre-amorphization implant was available by the XTEM calibrated TRIM calculation. Modification of the boron diffusion in the silicon and silicide is achieved by the multiple implants of Ge^+, C^+ and p-type doping.

References

[1] J.R. Brews, W. Fichtner, E.H. Nicolian, S.M. Sze, IEEE Electron Dev. Lett. EDL-1 (1980) 2.
[2] C. Dehm, J. Gyulai, H. Ryssel, Appl. Phys. Lett. 60 (1992) 1214.
[3] M. Togo, T. Mogami, K. Uwasawa, T. Kunio, VLSI Tech. Symp. 21 (1994).
[4] K. Takeuchi, T. Yamamoto, A. Furukawa, T. Tamura, K. Yoshida, VLSI Tech. Symp. 9 (1995).
[5] H. Jiang, C.M. Osburn, P. Smith, Z.-G. Xiao, D. Griffis, G. McGuire, G.A. Rozgonyi, J. Electron. Chem. Soc. 139 (1992) 196.
[6] M.C. Ozturk, J.J. Wortman, C.M. Osburn, A. Ajmera, G.A. Rozgonyi, E. Frey, W.K. Chu, C. Lee, IEEE Trans. Electron Dev. ED35 (1988) 659.
[7] S. Nishikawa, A. Tanaka, T. Yamaji, Appl. Phys. Lett. 60 (1992) 2270.
[8] P. Gas, V. Deline, F.M. d'Heurle, A. Michel, G. Scilla, J. Appl. Phys. 60 (1986) 1634.
[9] P. Gas, G. Scilla, A. Michel, F.K. LeGoues, O. Thomas, F.M. d'Heurle, J. Appl. Phys. 63 (1988) 5335.
[10] J. Sakano, S. Furukawa, Jpn. J. Appl. Phys. 32 (1993) 6163.
[11] C.Y. Lu, J.M. Sung, R. Liu, N.S. Tsai, R. Singh, S.J. Hillenius, H.C. Kirsch, IEEE Trans. Electron Dev. ED38 (1991) 246.
[12] A. Ohtomo, J. Ida, K. Yonekawa, K. Kai, I. Aikawa, A. Kita, K. Nishi, Jpn. J. Appl. Phys. 33 (1994) 475.
[13] J.P. Biersack, L.G. Haggmark, Nucl. Instrum. Meth. 174 (1980) 257.
[14] F.M. d'Heurle, J. Cotte, P. Gas, G. Goltz, C. Stanis, O. Thomas, Appl. Surf. Sci. 73 (1993) 167.
[15] S. Aronowitz, J. Appl. Phys. 68 (1990) 3293.